A Multiscale Approach to Modeling Plasmonic Nanorod Biosensors

THE JOURNAL OF PHYSICAL CHEMISTRY C

Article

pubs.acs.org/JPCC

A Multiscale Approach to Modeling Plasmonic Nanorod Biosensors

Tomasz J. Antosiewicz*[,†,‡] and Mikael Käll[‡]

[†]Centre of New Technologies, University of Warsaw, Banacha 2c, 02-097 Warsaw, Poland

[‡]Department of Physics, Chalmers University of Technology, SE-412 96 Göteborg, Sweden

ABSTRACT: Due to their strongly enhanced optical near-fields, plasmonic nanostructures are promising candidates as ultrasensitive label-free sensors of single molecule binding kinetics. However, the interpretation of nanoplasmonic sensing data is complicated by the spatial inhomogeneity of the near-field response and the stochastic nature of molecule-nanoparticle interactions, which makes it difficult to accurately count the number of adsorbed molecules per nanosensor. We combined electromagnetic calculations with stochastic diffusion-reaction simulations in order to investigate how these two sources of noise influence the uncertainty in measured molecular association and dissociation rate constants and concentration for the most common type of plasmonic nanosensor, the nanorod. Using this multiscale *in silico* tool, we show how to minimize the measurement uncertainty, and we identify the optimum nanorod aspect ratio for quantitative sensing.

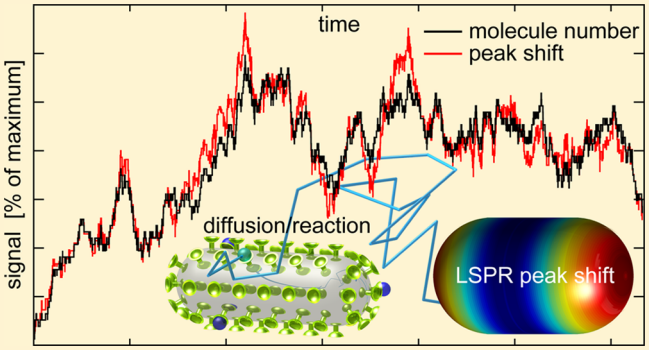

INTRODUCTION

All sensors are built around one common principle—to use a transduction mechanism to report on changes in the sensor environment. Regardless of whether the sensor is mechanical, electrical, or optical, the accuracy of the transduction mechanism is critical to achieving high fidelity performance. With the advent of nanotechnology, sensor miniaturization gained momentum and transduction devices with footprints below the micron scale have become a reality. A prominent position is occupied by various forms of optical sensors in the form of micro-[1] and nanosized[2,3] cavities and particles that allow for highly sensitive label-free detection.[4,5] Metal nanoparticles that support localized surface plasmon resonances (LSPRs) have been utilized in biosensing,[6] photodetection,[7] phase transition analysis[8] and spatial redistribution sensing.[9] The fields of chemistry, biology, and medicine offer some of the most exciting challenges and applications for such sensors, with the ultimate goal of detecting single small molecules[10] and measuring concentration over many decades.[11]

The usefulness of LSPRs in sensing as well as in other applications, like waveguiding[12] and solar harvesting,[13] stems from the fact that the collective excitation of the conduction electrons in the metal (plasmon) is accompanied by a resonantly enhanced electric near-field that is compressed to deeply subwavelength volumes.[14] The enhanced near-field causes any light-induced effects, such as light absorption,[15−17] fluorescence emission[18,19] and Raman scattering[11,20,21] to increase in efficiency. LSPR sensing utilizes the back-action from the dielectric residing in the enhanced near-field to the plasmonic nanostructure resonance, that is, a change in the dielectric response results in a shift of the LSPR wavelength. One can thus use the color spectrum of the nanostructure to measure small changes in the permittivity (or refractive index) of the environment.[22−26] The magnitude of the peak shift induced by a changing surrounding depends on factors such as nanoparticle shape, size, and constituent material.[27,28] Indeed, considerable efforts have gone into identifying which of these and other parameters are most important for ensuring good LSPR sensitivity.[29]

Colorimetric LSPR sensing is well suited for analysis of proteins, which typically have refractive indices approximately 10% larger than of water,[30] as well as many other biomolecules. Sensor specificity is then assured via functionalization of the sensor surface with receptors that target a specific analyte.[23,31] For many applications, it is enough to measure the ensemble-averaged response of a large number of nanoparticle sensors. The sensitivity can then be considerably better than one molecule per nanoparticle, and of the same order as that of classical planar film surface plasmon resonance (SPR) sensors.[32,33] However, an extension of the usefulness of LSPR sensing to measurements of single molecule binding reactions necessitates the establishment of a clear relation between the number of adsorbed molecules and the LSPR peak shift ($\Delta\lambda$). The problem can thus be formulated as a simple question: How does one make a reliable and accurate LSPR molecule counter? The nonuniform signal induced by the adsorption of a single molecule on a single nanostructure,[34,35] caused by the inherent inhomogeneity of the LSPR near-field, then becomes a prime

Special Issue: Richard P. Van Duyne Festschrift

Received: February 24, 2016
Revised: April 17, 2016
Published: April 21, 2016

DOI: 10.1021/acs.jpcc.6b01897
J. Phys. Chem. C 2016, 120, 20692−20701

concern. Indeed, under unfavorable conditions, for example, in the case of bow-tie dimers or sharp nanocones with electromagnetic hot spots, the variability of the local resonance peak shift may span more than 2 orders of magnitude, ranging from fractions of ångströms to single nanometers.[36] One must also consider the stochastic nature of molecular Brownian motion, and the fact that binding probablilities can vary across the surface of a nanostructure sensor. An additional complication is that the signal is subject to noise and drift that may potentially hide binding events generating small peak shifts. The accuracy of counting molecules, corresponding to the experimentally hard task of recording each binding event as it happens in real time,[37,38] then poses a nontrivial challenge. A closely connected and equally important problem is how to accurately measure binding rate constants and molecular affinities.[39] Association and dissociation rates can, in principle, be obtained by analyzing the temporal fluctuations of the equilibrium sensor signal,[40,41] but the extracted values can be expected to be distorted in the case of an inhomogeneous sensor response, thus compromising accuracy. Regardless of which quantity is being measured, concentration or rate constants, high accuracy typically implies prolonged monitoring of the peak shift of a given plasmonic resonator over time, well past the establishment of equilibrium. Multiplexing will, of course, aid in collection of statistically significant data in both cases.[42]

In an earlier work, we introduced a multiscale methodology that combines both aspects of molecular sensing via LSPR.[36] Here we build upon that methodology to minimize the uncertainty of measuring the number of adsorbed/bound molecules for a widely employed class of plasmonic nanosensors—plasmonic nanorods. Not only do we show that we can identify the geometry of a nanorod that maximizes the accuracy of the readout and explain its origin, but we also show a simpler yet equivalent method of performing the optimization without extensive numerical calculations. The paper is organized as follows: We begin by describing the methodology of combining the LSPR response with stochastic diffusion-reaction simulations. We then discuss the inhomogeneity of the plasmonic response, and the uncertainty it introduces, after which we analyze diffusion of molecules to the investigated sensors. We combine both parts into a single multiscale *in silico* experiment to address the uncertainty inherent to colorimetric sensors based on metallic nanorods and the question of how the shape of a nanorod sensor affects the accuracy of determining molecular rate constants. Finally, we discuss the origin of our observations and show how to minimize the uncertainty.

COMPUTATIONAL DETAILS

Two qualitatively distinct tools need to be combined to properly assess the considered problem.[36] First of all, the plasmonic response of nanorods upon binding of a small molecule has to be calculated. When light is polarized along the long axis of a nanorod, two hot spots, that is, regions of high field enhancement, appear at either end, while the field enhancement along the sides of the nanorod is comparatively weak. The field reacts to the presence of an object in close proximity to the nanorod, what results in a shift of the peak of the plasmon resonance. Here, we quantify the response of the LSPR to the binding of a molecule to investigate stochastic effects involved in single-particle plasmon sensing. The second part of our work deals with the stochastic nature of diffusion and binding reactions and their impact on LSPR sensing. For spherical nanoparticles far from a substrate (equivalent to a hemispherical particle on a substrate), diffusion does not affect sensing properties because molecules arrive uniformly at the surface of the sensor. However, as most metal nanoparticles used for sensing have complex shapes, diffusion causes an uneven distribution of molecules on the surface.[36] Furthermore, in microfluidic experiments, while not considered here, flow will similarly cause preferential binding to parts of the sensor. It is therefore important to consider both the electromagnetic aspects of single-particle plasmon sensing as well as the stochastic effects of mass transport to draw meaningful conclusions. Ultimately, the combination of a spatially inhomogeneous LSPR response and a spatially uneven binding probability affects the certainty of the measured signal and what it quantitatively represents, i.e. number of bound molecules and its error.

Figure 1a presents a scheme of a metal nanorod with an attached molecule, modeled as a dielectric sphere. In our

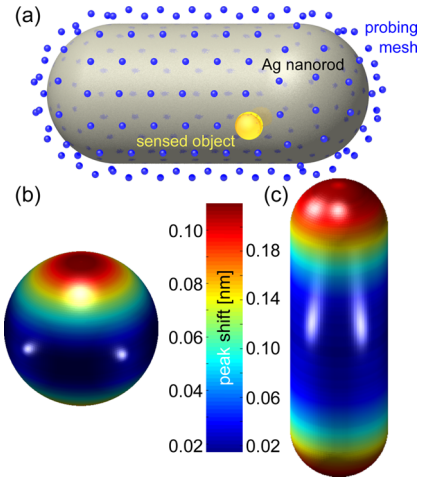

Figure 1. (a) Calculation of the LSPR shift induced by dielectric nanoparticle binding. The surface of a silver nanorod (length l) with hemispherical caps (radius r) is discretized into a semiregular mesh of a few hundred nodes (blue points). For a dielectric nanosphere (idealized molecule) positioned at each node, we calculate the extinction peak shift of the nanorod. (b,c) Each node is assigned the numerical value of the resonance shift and, when plotted in 3D, the mesh forms a peak shift map showing the spatial variation of the response of a given particle shape, in this case (b) a nanosphere (aspect ratio $A = 1$) and (c) a nanorod with $A = 3$.

investigations. we keep the volume of the metal resonator constant and vary its length and diameter by changing the rod's aspect ratio $A = l/2r$ from 1 to 4, where r is its radius and l is its length including both hemispherical caps. The volume is fixed to that of a nanosphere (nanorod with $A = 1$) with $r = 30$ nm. The dielectric sphere has a radius of 3 nm and a refractive index of 1.5. The metal is modeled using the Drude permittivity function $\epsilon(\omega) = \epsilon_\infty - \omega_p^2/(\omega(\omega + i\gamma))$, where the parameters are $\epsilon_\infty = 3.7$, $\hbar\omega_p = 8.55$ eV, and $\hbar\gamma = 130$ meV and are close to that of silver. Incident light is polarized along the length of the nanowire. To calculate peak shifts, $\Delta\lambda$, induced by a binding molecule at various locations on the surface of the Ag resonator, we use the finite difference time domain (FDTD) method with a mesh size of 0.5 nm. We discretize the surface of the nanorod into a regular mesh of positions at which we place the dielectric sphere, calculate its effect on the extinction

DOI: 10.1021/acs.jpcc.6b01897
J. Phys. Chem. C 2016, 120, 20692−20701

spectrum, and assign the peak shift's numerical value to that particular point in space. Once done for all selected points, this gives a three-dimensional (3D) sensitivity map of binding of the model molecule (dielectric nanosphere). In Figure 1b,c we show two exemplary cases for $A = 1$ and 3, respectively. While maximum peak shifts are larger for the longer structure due to greater field enhancements at either end and refractive index sensitivity is known to increase with aspect ratio,[43] that does not necessarily translate into smaller uncertainty when sensing single molecules.

The sensing experiment is carried out by combining diffusion of noninteracting molecules in a volume occupied by a plasmonic resonator with binding/unbinding reactions at its surface; a detailed description is found elsewhere.[36] Briefly, diffusion of molecules is modeled as a Wiener process in which the mean one-dimensional (1D) diffusion length is $s = \sqrt{2D\Delta_t}$, where $D = 10\ \mu m^2/s$ is the diffusion constant and Δ_t is a time interval. To obtain a random 3D translation of a diffusing molecule, three random numbers are drawn from the (0,1) normal distribution and multiplied by s. As a molecule diffuses, it may encounter a receptor attached to the surface of the resonator. This initiates a probabilistic evaluation of its chance to bind. This probability P_b depends on the association reaction rate $k_a = 10^6\ M^{-1}\ s^{-1}$, the distance between the molecule and nearby receptors, as well as the employed time step, according to $P_b = 1 - \exp(-\Delta_t \sum_i (k_a/V_i))$. Here, V_i is a spherical volume given by the distance between the molecule and a receptor and the sum runs over all free receptors closer than a reaction radius of 10 nm. Should binding occur, the molecule ceases to move until it unbinds with a rate $k_d = 0.005\ s^{-1}$. These rates are based on considerations of reaction kinetics explored in biosensing.[44] $\Delta_t = 100$ ns assures a small enough s that the surface of the resonator is probed accurately and molecules resolve all details of the rods.[36] We perform diffusion-reaction simulations at four molecular concentrations $\rho = 0.25$ pM, 5 pM, 100 pM, and 2 nM in the presence of nanorods with aspect ratios of 1, 1.5, 2, and 4. The numerical experiments run for 10 000 s and are repeated to gather at least 50k binding events for every combination of A and ρ to ensure adequate statistics.

RESULTS AND DISCUSSION

Inhomogenity of the Plasmonic Response. While a lot of work has been carried out on the optical properties of nanorods, here we analyze them in a different context than before. Having obtained all 3D sensitivity maps, we calculate the average peak shift $\overline{\Delta\lambda}$ and its standard deviation σ. Because each rod has a different range of viable peak shifts, in Figure 2 we plot the ratio of $\overline{\Delta\lambda}$ to σ, which in essence is a sensor quality factor $Q \equiv \overline{\Delta\lambda}/\sigma$, as a function of A; this is equivalent to having exactly one molecule ($N = 1$) bound to the surface of the rod in a random position. We see that for increasing A, the Q-factor increases until it reaches a maximum at $A = 1.5$. Subsequently, for larger A the Q-factor decreases. The maximum is significant in that it represents the lowest possible uncertainty of a peak shift measurement for this class of sensors. It persists when the number of molecules increases and, while Q spans an increasing range of values with increasing N, the relative amplitude of the maximum remains constant.

The origin of this maximum stems from the spatial dependence of the peak shifts for each rod. Figure 3a shows a frequency analysis of the peak shift maps with $\Delta\lambda$ normalized

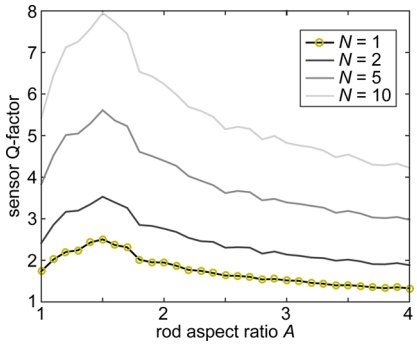

Figure 2. Sensor quality factor Q as a function of rod aspect ratio A calculated for an exact number of molecules bound to a rod. We assume each receptor has an equal binding probability. A maximum for $A = 1.5$ is observed, indicating an optimum rod aspect ratio from the response uncertainty point of view. It persists when we increase the exact number of molecules on the surface of the nanorod.

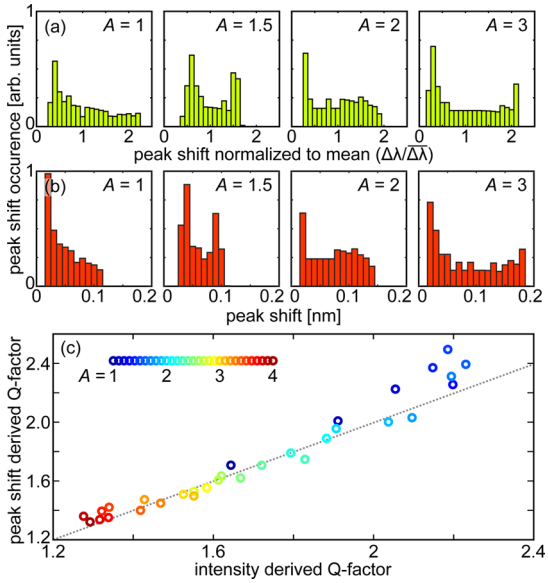

Figure 3. (a) Normalized peak shift distributions ($\Delta\lambda/\overline{\Delta\lambda}$) for rods of various aspect rations A. (b) Absolute peak shift (in nm) distributions. The distributions are broad and flat with a maximum at low peak shifts. The narrowest peak shift distribution is for $A = 1.5$ and is the reason behind the maximum of the sensor Q-factor plotted in Figure 2. The normalization in each plot in the top row is to their respective mean values. (c) Peak-shift-derived Q-factor vs intensity-enhancement-derived Q-factor, note the almost linear 1:1 dependence. Each circle represents a particular A.

to their respective mean values, while in Figure 3b corresponding absolute peak shift values are shown. These distributions are non-Gaussian, flat with local maxima positioned at small peak shift values, and are the reason for the large uncertainty and resulting Q-factor dependence plotted in Figure 2. The dependence of the uncertainty on the aspect ratio is caused by a variation of their width. It is clear from Figure 3 that the narrowest distribution occurs for $A = 1.5$, the value at which Q is the largest (inverse dependence on σ), while for both larger and smaller values of the aspect ratio, the width of the distributions is larger.

LSPR shifts are caused by the appearance of a target molecule near the surface of a sensor. The electromagnetic field at that location interacts with the sensed object altering the

DOI: 10.1021/acs.jpcc.6b01897
J. Phys. Chem. C 2016, 120, 20692−20701

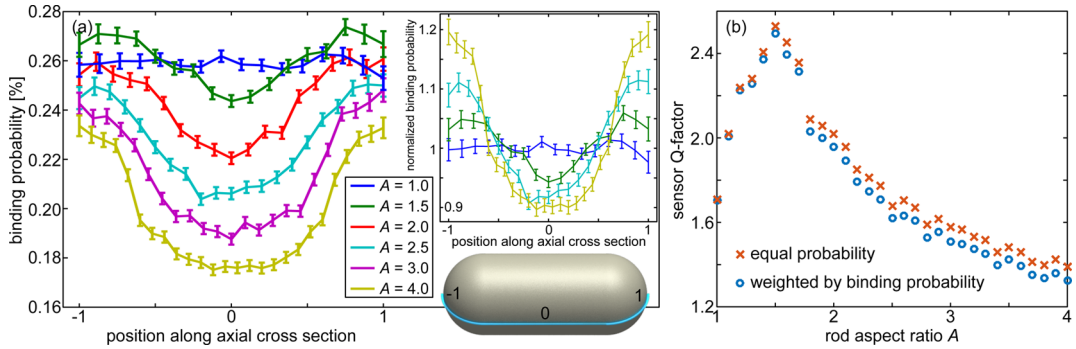

Figure 4. (a) Single molecule binding probability to receptors positioned on nanorods with selected aspect ratios A. For A = 1, the probability is uniform. As A increases, the probability at the center of the nanorod (position 0) decreases in comparison to that at either end. The inset replots this using a normalized scale to show by how much the binding probability deviates from a flat one. The blue line on the surface of the nanorod marks the cross section along which we plot the probability. (b) Comparison of Q-factors of peak shifts weighted by a flat probability (circles) and by the single molecule probability (crosses).

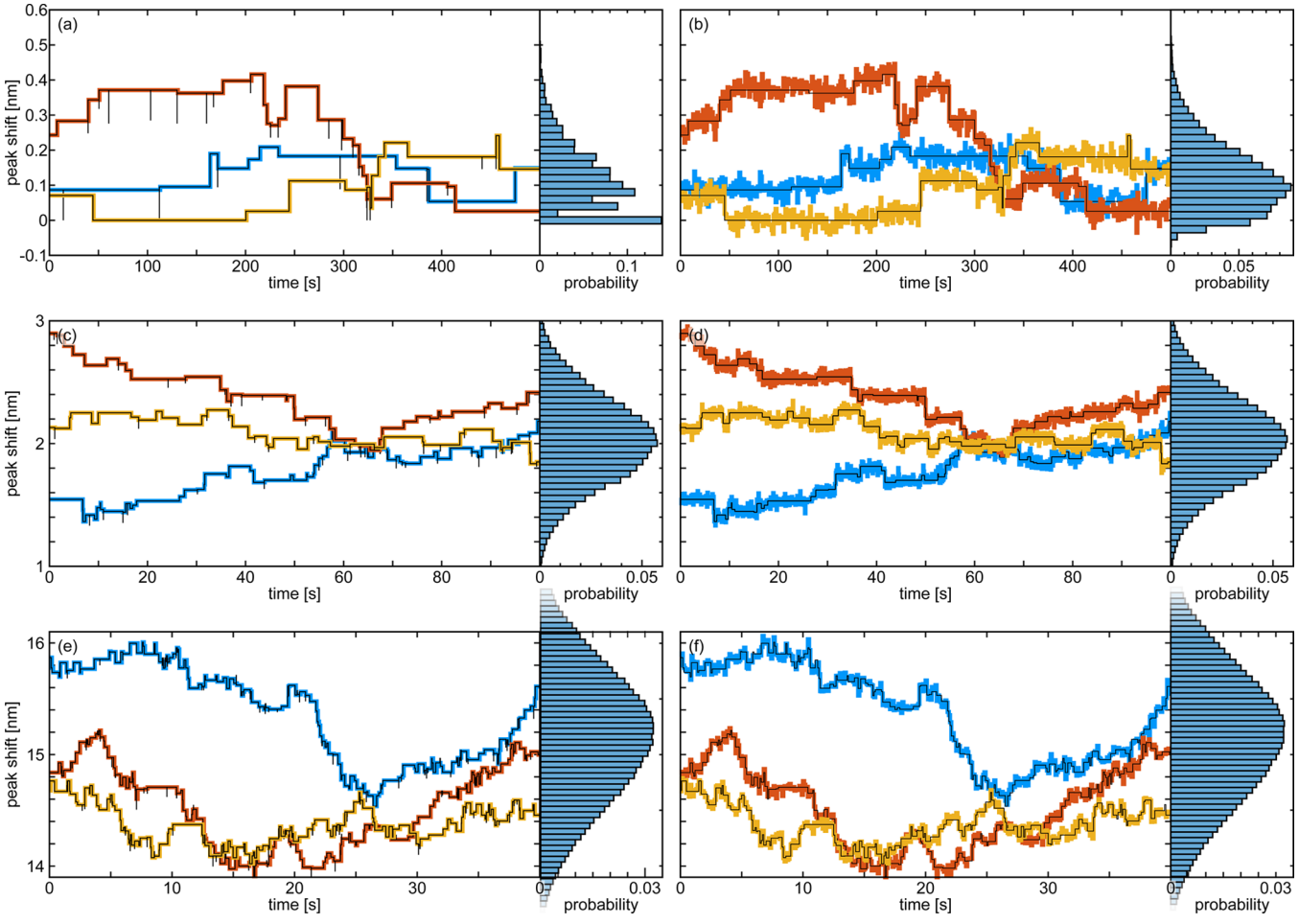

Figure 5. Three representative $\Delta\lambda$ time traces for (a,b) ρ = 5 pM, (c,d) 100 pM, and (e,f) 2 nM with peak shift probability histograms for A = 1.5. In the left column the thick colored lines represent time traces sampled at 1 s for ρ = 5 pM and 100 ms for 100 pM and 2 nM, while the thin black lines show the simulated time traces with all events. The vertical thin black lines mark rapid rebinding events, which occur on time scales shorter than the sampling rate. If the molecule binds at a different receptor, this is registered as a step of the peak shift trace which, without access to detailed information, is interpreted as a change of the number of attached molecules. In the right column, the colored lines show the sampled time traces with added white noise and the black lines denote the sampled time trace without noise. Note the loss of many unbinding events even for low concentrations and an increasing number of binding events with increasing ρ.

resonance conditions and inducing a slight shift of the extinction peak. In Figure 3c, we plot the relation between the Q-factors calculated from peak shifts and the intensity enhancement factors M^2 ($M^2 \equiv |E|^2/|E_0|^2$, where E and E_0 are the total local and incident electric fields, respectively). This relation is approximately linear, which means that, at least in the case of the rods considered here, it is enough to analyze the standard deviation of the field enhancement at locations at

DOI: 10.1021/acs.jpcc.6b01897
J. Phys. Chem. C 2016, 120, 20692−20701

which the analyte binds. Such an analysis, while simple and rapid in comparison to simulating the LSPR response to molecule binding, is enough to identify the Q-factor and thus the peak shift uncertainty of a considered structure. It is, however, important to note that, while the general trend between the $\Delta\lambda$ and the M^2 derived Q-factors is linear, there is considerable spread, especially for probes placed in the high intensity regions. Part of this scatter may be caused by discretization errors of the calculations themselves; however, in part it is caused by a deviation from the linearity between M^2 and $\Delta\lambda$.[25]

Diffusion of Molecules to Nanorods. The first molecule that binds to a sensor is, in principle, free to attach to any receptor at its surface. Subsequent arrivals, while also exhibiting the same diffusion profile, may only bind to free receptors. Hence, the probability of binding to a particular spot depends on all previous binding events. To be able to quantify this aspect of molecule sensing, we first investigate single-molecule binding (when the surface of the rod is free initially) and then turn to the impact of partial surface coverage.

Figure 4a shows the single-molecule binding probability to rod-shaped sensors (in solution) for increasing aspect ratios under the assumption that a single receptor occupies ca. a 6 nm by 6 nm patch, which is matched to the size of the probing molecule (3 nm radius). Due to the cylindrical symmetry of the sensors, the probability is plotted along the length-wise cross section marked by a blue line in the inset. As noted before, the probability for a sphere is flat. With an increase of A, two things occur: (i) the average probability decreases due to an increasing surface area and, consequently, a larger number of receptors, and (ii) at the ends of the rods, the binding probability increases above the corresponding average at the expense of a lower probability near the center. This is clearly demonstrated in the inset in which the binding probability is normalized to the corresponding average. For long rods, molecules are 30% more likely to bind to the receptor with the highest sensitivity than to the one with the lowest.

As large as this variability of the binding probability is, it turns out to only slightly affect the uncertainty of the readout. In Figure 4b, we plot the Q-factors for a hypothetical flat binding probability (circles) and for the single-molecule probabilities (depicted in Figure 4a) with crosses. For small rods with $A \leq 1.5$, for which the binding probability deviates only slightly from being uniform, the difference in uncertainty is almost negligible. The difference then increases slowly as the rods get longer. However, the calculated difference is less than 10% even for the longest rods considered ($A = 4$). At a qualitative level, incorporation of the binding probability is equivalent to removing a small number of receptors from the middle of the rod (low sensitivity part) and moving them to the caps (high sensitivity areas). This change to the peak shift distribution (c.f. Figure 3a,b) mainly increases the mean peak shift of rods (at most 8% for $A = 4$), but leaves the standard deviation almost unaltered. With the Q-factor defined as the ratio of these two values, it is reasonable that Q increases marginally. Thus, for these types of sensors, the single molecule stochastic properties of the LSPR response are adequate in minimizing the readout uncertainty. However, this may not be the case for more complicated nanoplasmonic structures, and, for certain nanosensor geometries, the binding probability will need to be considered.

Plasmonic-Diffusion-Reaction Experiment *in Silico*. In each row in Figure 5, we have plotted three exemplary time traces of $\Delta\lambda$ for rods with $A = 1.5$ for different ρ. The left panels (Figure 5a,c,e) present time traces sampled at 1 s (top, 5 pM) and 100 ms (middle and bottom with 100 pM and 2 nM, respectively) − these are shown with thick colored lines−and traces with all events as thick black lines. Additionally, in the right panels we compare pure sampled traces with ones with added white noise (standard deviation of 0.02 nm, 1 s sampling, and 0.03 nm for 100 ms, comparable to experimental noise[9]). The time windows are chosen so that single events are easily discernible. We also plot probability histograms of measuring a given peak shift value, whose Q-factors, shown in Table 1, are a measure of the uncertainty.

Table 1. Q-Factor of the Sensors as Functions of Molecular Concentration ρ and Rod Aspect Ratio A As Derived from Time Traces

	aspect ratio A			
ρ	1	1.5	2	4
5 pM	1.20	1.29	1.26	1.25
100 pM	3.57	4.00	3.84	3.84
2 nM	15.2	17.5	17.2	15.2

The time traces in Figure 5 show considerable variation around the mean value. Large single steps, which are easy to identify, account for only a fraction of all events, while some bindings or unbindings may not show because of noise. Also, rapid rebinding is not measured since the time scales of these processes are below the sampling rate. These rapid events, which are marked by thin vertical black lines in the left column of Figure 5, do not show up in the measured time trace and thus are not included in subsequent analysis. Moreover, since rapid rebinding may result in a molecule binding at a different receptor, the observed peak shift step may be falsely attributed to a change in the number of bound molecules. These rapid events, as well as the variability of peak shift magnitude, pose a challenge in the correct interpretation and analysis of experimental as well as our simulated data. The result is that, without prior knowledge of the achievable response range and probabilities, it is quite difficult to confidently ascertain the number of molecules causing a particular peak shift when dealing with only a short measurement. An even worse case is when the signal is measured at only a single point in time, as there is no way of distinguishing a single bound molecule from a number of them causing an identical peak shift. The probability of such an event occurring depends on the sensor in question and the lower it is, the better is the sensor at measuring concentration. For the traces in Figure 5 the worst case is for 5 pM. The simulated signal is 0.15 ± 0.12 nm which, if used to measure concentration, would yield uncertainties on the order of the measured signal. For the larger concentrations of $\rho = 100$ pM and 2 nM, the uncertainty decreases to ca. 25% and 6% of the measured value, respectively. The Q-factors, inversely proportional to the uncertainty, are shown in Table 1. While the increase of the Q-factor with ρ is the result of Poissonian characteristics of binding events[42,45] (for small coverages when the assumption on independence of bindings holds), in all cases the largest Q-factors are measured for $A = 1.5$.

In addition to determining the mean and standard deviation of $\Delta\lambda$ as measures of concentration, it is also possible to use the time traces to determine the rate constants.[40,41] The temporal fluctuations of N and $\Delta\lambda$ (see Figure 6a) are Fourier

DOI: 10.1021/acs.jpcc.6b01897
J. Phys. Chem. C 2016, 120, 20692−20701

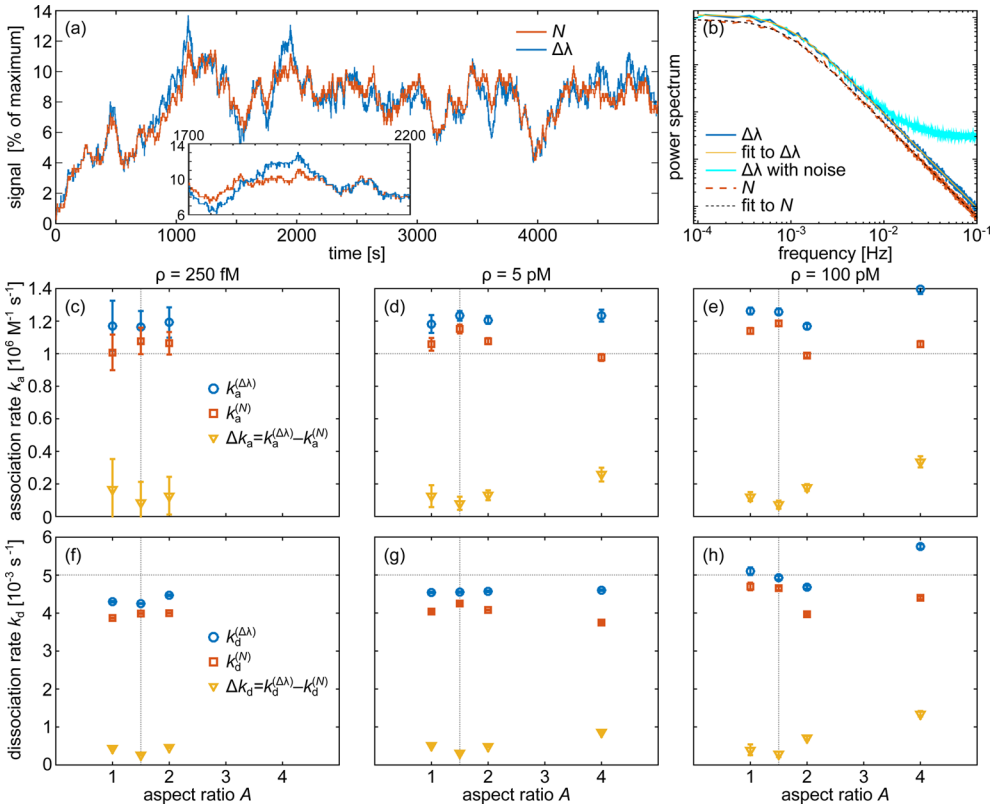

Figure 6. (a) Comparison of a time trace of receptor occupancy (N) and the corresponding peak shift ($\Delta\lambda$) normalized to maximum possible values for A = 1 and ρ = 100 pM; the inset shows a magnification of the fluctuations. (b) Mean power spectrum of equilibrium fluctuations for receptor occupancy and peak shifts with fitted dependence; power spectrum of peak shift traces with noise. (c–h) Calculated association and dissociation rate constants from receptor occupancy and peak shift time traces. Circles – $k^{(\Delta\lambda)}$, squares – $k^{(N)}$, triangles – Δk, calculated for association and dissociation. Rates calculated from peak shifts are more inaccurate than those from receptor occupancy and the magnitude of the difference (triangles) is inversely proportional to the Q-factor of the sensors plotted in Figure 2. The dotted horizontal and vertical lines mark the true rates and the best accuracy, respectively.

transformed to yield a frequency spectrum (Figure 6b), and the time constant τ of the resulting distribution is obtained by fitting a Lorentzian function $f(\nu) = c\tau/(1 + (2\pi\nu\tau)^2)$ with ν being the frequency and c a fitting parameter. The rate constants are calculated from τ and the mean equilibrium coverage $\bar{x}$ ($x \equiv \Delta\lambda$ or N and indicates a peak shift or occupancy derived value) as $k_a^{(x)} = \bar{x}/(\tau\rho)$ and $k_d^{(x)} = \tau^{-1} - k_a^{(x)}\rho$. Figure 6b also shows in cyan a typical power spectrum of a noisy $\Delta\lambda$ signal, whose flat tail depends on the noise level. However, this type of analysis is quite robust and can deal with signal-to-noise levels on the order of unity or less.[40]

The fluctuation-approach may be used when the surface coverage is smaller than 10% due to a large deviation from the Langmuir adsorption model (in ref 40 this was extended to 20% with a modified time constant),[40,41] which in our case means that the 2 nM case needs to be excluded. Instead, we use data from simulations with ρ = 0.25 pM. Having access to both the temporal evolution of the number of adsorbed molecules as well as the resulting peak shifts, we analyzed both to highlight how the sensitivity inhomogeneity affects the measurement. We should note here, that the rates plotted here were calculated from time traces with a 1 ms sampling rate. This means that any rapid rebinding events at the same receptor are not taken into account at all, while those that rebind at a different receptor and cause a peak shift have an impact only on the peak shift analysis.

Figure 6c–h presents the calculated association and dissociation rate constants. Recalling the assigned values in our stochastic simulations, $k_a = 10^6$ M^{-1} s^{-1} and $k_d = 5 \times 10^{-3}$ s^{-1}, we obtain relatively good agreement in both cases. k_a derived from the molecule count is overestimated on average by 10%. When this parameter is obtained from the peak shift fluctuations, it is at least 20% larger than the set value. Looking at the bare k_a values, it is not possible to identify the details of the impact of the peak shift inhomogeneity (aside from an increased deviation) on the measurement of the rate. Only when looking at the difference $\Delta k_a \equiv k_a^{(\Delta\lambda)} - k_a^{(N)}$ does the trend become clear. It follows inversely the dependence of the sensor Q-factor versus the aspect ratio of the rods, as plotted in Figure 2. For A = 1.5, this increase is the smallest, resulting in an association rate constant overestimated by less than 10%, while for other considered aspect ratios the accuracy is worse. This increase of the peak shift derived rate relative to the molecule number derived one is the result of the "noise" of the plasmonic response. The power spectrum (Figure 6b) of the $\Delta\lambda$ time trace is wider than that of N, which is explained by the fact that more high-frequency components are contained within the "noisier" signal. The wider Lorentzian then implies larger rates.

The dissociation rate constant is calculated to be, overall, smaller than its assigned value of 0.005 s^{-1}. The cause of this is the possibility of rapid rebinding, which occurs over time scales faster than the readout[46] (see, e.g., the red trace in Figure 5a).

DOI: 10.1021/acs.jpcc.6b01897
J. Phys. Chem. C 2016, 120, 20692–20701

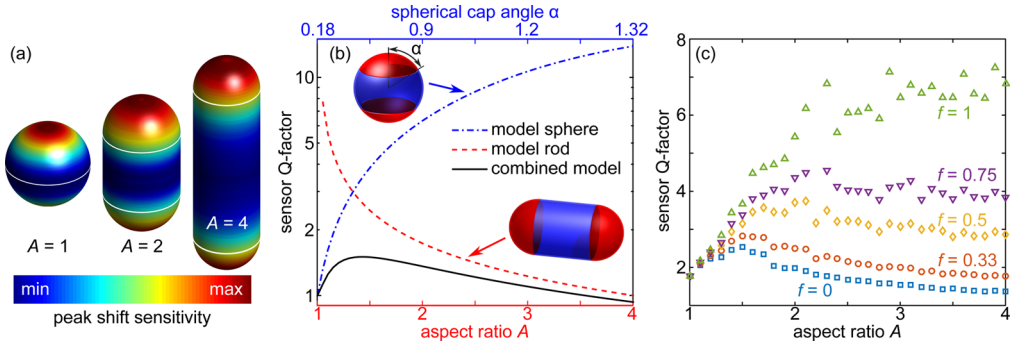

Figure 7. (a) Evolution of peak shifts with aspect ratio A. There are two categories of changes: with an increasing A, the sensitivity distribution at the caps (marked with thin white lines) becomes more homogeneous while the area at the sides of the rods, which exhibits low sensitivity, increases approximately linearly. (b) Sensor Q-factors for a model digital (0/1) peak shift distribution for a rod (dashed line) and a sphere (dash-dotted line). For the rod the peak shift is 1 (red) at its caps and 0 (blue) at its center; as A increases so does the area with 0 peak shift and as a result the Q-factor decreases. To model the caps we use a sphere with a flexible split between a peak shift of 1 and 0 via parameter α; as α increases so does Q, α is the angle for which the peak shift at the cap is at least 80% of maximum for a given A. The combined effect of both gives the measured dependence of Q seen in Figure 2. (c) Rod Q-factor as a function of rod aspect ratio A calculated for the case when a fraction f of the side of the rod is blocked from binding. For $f = 0$ (squares), all receptors can bind molecules and the Q is then small (signal uncertainty is large). With half of the receptors on the rod side passivated (starting from the middle), the Q-factor for large A is relatively constant. When $f = 1$, and only the caps remain active, Q is up to 5 times larger than for the whole rod.

The measured rate is a function of the rebinding probability, which depends on the local properties of the resonator and association rate constants and in our case is approximately 10−20%. Such a lowering of the rate is in fact obtained from our calculations, as is clearly seen for $k_d^{(N)}$. The dissociation rate calculated based on the peak shift time trace, like $k_a^{(\Delta\lambda)}$, is larger compared to the receptor occupancy-derived values for the A = 1.5 rod showing the smallest increase, similar to the behavior observed in Figure 2.

Tailoring the Signal Uncertainty. The final question we consider is the reason for the observed dependence of the Q-factor (i.e., signal uncertainty) for the investigated rods. To this end we qualitatively analyze the peak shift maps of the rods, three of which are plotted in Figure 7a. The uniformity of the sensitivity varies strongly with A, as discussed above. For A = 1, only the top and bottom of the sphere have large peak shifts while the equator region exhibits low sensitivity. A larger A causes the homogeneous field inside a sphere to deviate from being parallel to the long axis, and, at the nanorods' caps, the field lines become more perpendicular to the surface. This causes the field enhancement and sensitivity to increase. At the same time the fields are still relatively parallel to the surface of the cylindrical part and there the field enhancement is low. This is evident for the rod with A = 2, whose low sensitivity region has all but moved to the sides while the caps now generate a peak shift that is at least 50% of the maximum value reached at the apex. Increasing A to 4 makes the caps' response even more uniform, with peak shifts of at least 70% of the maximum. Simultaneously, increasing A causes the cylindrical part with small peak shifts to increase in length.

The impacts on Q of these two effects caused by increasing A are easily elucidated by considering two limiting cases. The first one is a rod whose caps have a sensitivity of 1 and whose side has 0 sensitivity (see cartoon in Figure 7b) an assumption appropriate for long rods with quasi-uniform hot spots at the caps and low sensitivity at their sides. Calculating Q yields a monotonically decreasing function with A (dashed red line), exactly what is observed for the actual peak shifts in the limit of $A > 2$. However, for $A \lesssim 2$ the caps can not be considered as having a uniform peak shift. Thus, the second limiting case is that of a sphere whose surface is split into two domains, one with a peak shift of 1, the other with 0, this corresponding to a rod in which we completely neglect the cylindrical part. The parameter defining the split is the angle α (see Figure 7b). As α increases (a nonlinear dependence on A derived from FDTD calculations assuming that the peak shift is at least 80% of the maximum value) the sphere (cap) peak shift becomes more homogeneous and the Q-factor increases (dash-dotted blue line). The combined effect of the two contributions gives the behavior calculated for the actual peak shift maps.

This interpretation serves as a guide to decrease the sensing uncertainty of rods. This can be done by blocking[38] a fraction f of the nanorod's side (Figure 7c) from molecular binding. For no blocking ($f = 0$), Q is unchanged. With partial blocking, f = 0.5, Q for large aspect ratios increases 2-fold. The largest increase is observed for f = 1, when only the rod's caps participate in binding. The Q-factor is then enhanced 5-fold, meaning that measured $\Delta\lambda$ will be ascribed to a more precise number of molecules. For small aspect ratios $A \leq 1.5$, the uncertainty is not affected significantly since for these rods the caps constitute a large part of their surfaces. Blocking receptors at the sides causes the low sensitivity parts to stop contributing to sensing and effectively makes the peak shift distribution (cf. Figure 3a,b) narrower by removing their left sides. Effectively, the standard deviation of the distributions decreases, the mean peak shift increases, and consequently Q increases. One can also note the difference between the trace for f = 1 and the dependence for the model sphere in Figure 7, with Q being smaller for the passivated rod. The reason is that the remaining inhomogeneity of the real caps' response which, while getting smaller for increasing A, does not reach a δ-distribution. If passivation would also encompass part of the caps (near the side), then Q would become even larger with a theoretical limit of infinity for the case of only one receptor per nanorod (perfect precision). However, in this case the reactive area would be small, and the resonator would be less likely to detect a molecule, not to mention that such a (single) nanorod could only act as a yes/no type of detector rather than as a concentration sensor. More importantly, a small number of binding sites would significantly limit the possibility of

DOI: 10.1021/acs.jpcc.6b01897
J. Phys. Chem. C 2016, 120, 20692−20701

measuring binding rates. Thus, one needs to carefully weigh the acceptable uncertainty of the signal against the sensing range.

CONCLUSIONS AND SUMMARY

With increasing use of plasmonic nanoparticles to sense low numbers of molecules, it is ever more important to address their limitations. An important problem faced by these sensors is the inhomogeneous response that affects the uncertainty (here expressed as a sensor Q-factor) in determining the number of molecules attached to the nanoparticle. For example, in the recent study of Brulé et al.[11] in which SERS was used to measure molecular concentration the uncertainty was significant. With regards to the colorimetric approach, a recent study addressed the inhomogeneity of the LSPR response to optimize a disk-[47] or rod-shaped[48] sensor, although without explicitly taking into account the stochastic nature of binding for a disk or employing a quasi-static continuum model to describe interactions between plasmons and nonabsorbing molecules.[45]

The two sources of uncertainty—the inhomogeneous LSPR response and stochastic effects—are not completely independent of each other. So while the optical and stochastic properties can be analyzed independently, one has to keep in mind that the shape of the plasmonic resonator affects both the local field enhancement (and thus sensitivity) and the binding probability. To design an accurate sensor, one has to factor into account both effects. In principle, however, the most important one is the LSPR response, because stochasticity, i.e. the Poissonian characteristics of the number of binding events,[42,45] is unavoidable and will add to the uncertainty caused by the inhomogeneous peak shift distribution. It is also necessary to remember that diffusion also results in preferential binding to some parts of a nonspherical sensor. However, as shown here for the case of nanorods, even 30% differences in the binding probability between the center of a rod and its end change only slightly the uncertainty caused by an inhomogeneous LSPR response. Nevertheless, other sensor shapes may be affected to a much greater degree and at least a perfunctory analysis of the binding probability profile should be attempted.

In the case of nanorods, the most important factor that can be controlled is the intensity enhancement distribution, which can be tuned by the geometry of the resonator. The investigated nanorods, while often being used as plasmonic biosensors, are in their basic form not the best candidates because, for low numbers of attached molecules, the errors are on the order of the measured number. A nanorod with the best accuracy can be identified through an analysis of the spatial distribution of the peak shift (or, equivalently, the intensity enhancement distribution). It then turns out that the optimum aspect ratio is $A = 1.5$. Removing or blocking receptors residing on the low sensitivity midpart of a nanorod from molecular attachment or selective attachment to high sensitivity hot-spots can further increase the accuracy.[38,49,50] This effect is more pronounced the longer the nanorod becomes, although at least 75% of the cylindrical part of the rod has to be passivated to generate a substantial improvement. However, passivation, while beneficial from the point of view of increasing the accuracy of counting molecules, simultaneously decreases the working range of the sensor: the smaller the number of available receptors, the narrower the dynamic range. This limitation can be overcome by increasing the number of active sensors per given surface area. However, potential drawbacks include the need to monitor many nanoparticles simultaneously and inhomogeneous response of resonators, which are rarely identical.

In summary, we have shown how to use a multiscale approach utilizing electromagnetic calculations and stochastic diffusion-reaction simulations to minimize the readout uncertainty of functionalized plasmonic molecular sensors. This minimization is equivalent to maximizing a plasmonic sensors' Q-factor, which is the ratio of the mean and standard deviation of the peak shift. The three factors influencing the accuracy of such sensors are the inhomogeneity of the plasmonic response and the spatial binding probability, both affected by the sensor shape, as well as the stochastic properties of receptor occupancy. We applied this methodology to study the uncertainty of counting molecules using a typical plasmonic sensor—the nanorod—as a function of its aspect ratio. We also quantified the magnitude of the error in calculating molecular rate constants from equilibrium fluctuations of the peak shift vs receptor occupancy. A clear minimum was identified for an aspect ratio of 1.5, with both shorter and longer rods exhibiting worse results. This is especially important for long rods, whose large maximum peak shifts may offer clearer yes/no answers, but may fail at accurate counting of bound molecules (and consequently measuring molecular concentration). For these types of nanorods, it is critical to passivate parts of their surface area to ensure a more uniform response to the presence of the analyte. However, given the multitude of metal nanoparticles, it is still an open question how to realize an optimum molecule counting scheme with plasmonic nanoparticle sensors, especially when partial passivation of the sensor's surface is considered.

AUTHOR INFORMATION

Corresponding Author

*E-mail: tomasz.antosiewicz@uw.edu.pl; Phone: +48 22 55 43679.

Notes

The authors declare no competing financial interest.

ACKNOWLEDGMENTS

This work was supported by the project 2012/07/D/ST3/02152 awarded by the Polish National Science Center and the Swedish Foundation for Strategic Research.

REFERENCES

(1) Foreman, M. R.; Swaim, J. D.; Vollmer, F. Whispering Gallery Mode Sensors. *Adv. Opt. Photonics* **2015**, *7*, 168−240.
(2) Tong, L.; Wei, H.; Zhang, S.; Xu, H. Recent Advances in Plasmonic Sensors. *Sensors* **2014**, *14*, 7959−7973.
(3) Sriram, M.; Zong, K.; Vivekchand, S. R. C.; Gooding, J. J. Single Nanoparticle Plasmonic Sensors. *Sensors* **2015**, *15*, 25774−25792.
(4) Fan, X.; White, I. M.; Shopova, S. I.; Zhu, H.; Suter, J. D.; Sun, Y. Sensitive Optical Biosensors for Unlabeled Targets: A Review. *Anal. Chim. Acta* **2008**, *620*, 8−26.
(5) Hunt, H. K.; Armani, A. M. Label-Free Biological and Chemical Sensors. *Nanoscale* **2010**, *2*, 1544−1559.
(6) Anker, J. N.; Hall, W. P.; Lyandres, O.; Shah, N. C.; Zhao, J.; Van Duyne, R. P. Biosensing with Plasmonic Nanosensors. *Nat. Mater.* **2008**, *7*, 442−453.
(7) Chalabi, H.; Schoen, D.; Brongersma, M. L. Hot-Electron Photodetection with a Plasmonic Nanostripe Antenna. *Nano Lett.* **2014**, *14*, 1374−1380.
(8) Appavoo, K.; Lei, D. Y.; Sonnefraud, Y.; Wang, B.; Pantelides, S. T.; Maier, S. A.; Haglund, R. F. Role of Defects in the Phase Transition

DOI: 10.1021/acs.jpcc.6b01897
J. Phys. Chem. C 2016, 120, 20692−20701

of VO_2 Nanoparticles Probed by Plasmon Resonance Spectroscopy. *Nano Lett.* **2012**, *12*, 780−786.
(9) Tabib Zadeh Adibi, P.; Mazzotta, F.; Antosiewicz, T. J.; Skoglundh, M.; Grönbeck, H.; Langhammer, C. In Situ Plasmonic Sensing of Platinum Model Catalyst Sintering on Different Oxide Supports and in O_2 and NO_2 Atmospheres with Different Concentrations. *ACS Catal.* **2015**, *5*, 426−432.
(10) Baaske, M. D.; Foreman, M. R.; Vollmer, F. Singe-Molecule Nucleic Acid Interactions Monitored on a Label-Free Microcavity Biosensor Platform. *Nat. Nanotechnol.* **2014**, *9*, 933−939.
(11) Brulé, T.; Bouhelier, A.; Yockell-Leliévre, H.; Clément, J.-E.; Leray, A.; Dereux, A.; Finot, E. Statistical and Fourier Analysis for In-line Concentration Sensitivity in Single Molecule Dynamic-SERS. *ACS Photonics* **2015**, *2*, 1266−1271.
(12) Saj, W. M.; Antosiewicz, T. J.; Pniewski, J.; Szoplik, T. Energy Transport in Plasmon Waveguides on Chain of Metal Nanoplates. *Opto-Electron. Rev.* **2006**, *14*, 243−251.
(13) Clavero, C. Plasmon-Induced Hot-Electron Generation at Nanoparticle/Metal-Oxide Interfaces for Photovoltaic and Photocatalytic Devices. *Nat. Photonics* **2014**, *8*, 95−103.
(14) Kristensen, P. T.; Hughes, S. Modes and Mode Volumes of Leaky Optical Cavities and Plasmonic Nanoresonators. *ACS Photonics* **2014**, *1*, 2−10.
(15) Aydin, K.; Ferry, V. E.; Briggs, R. M.; Atwater, H. A. Broadband Polarization-Independent Resonant Light Absorption Using Ultrathin Plasmonic Super Absorbers. *Nat. Commun.* **2011**, *2*, 517.
(16) Antosiewicz, T. J.; Apell, S. P.; Wadell, C.; Langhammer, C. Absorption Enhancement in Lossy Transition Metal Elements of Plasmonic Nanosandwiches. *J. Phys. Chem. C* **2012**, *116*, 20522−20529.
(17) Kim, K.-J.; Chong, X.; Kreider, P. B.; Ma, G.; Ohodnicki, P. R.; Baltrus, J. P.; Wang, A. X.; Chang, C.-H. Plasmonics-Enhanced Metal-Organic Framework Nanoporous Films for Highly Sensitive Near-Infrared Absorption. *J. Mater. Chem. C* **2015**, *3*, 2763−2767.
(18) Tam, F.; Goodrich, G. P.; Johnson, B. R.; Halas, N. J. Plasmonic Enhancement of Molecular Fluorescence. *Nano Lett.* **2007**, *7*, 496−501.
(19) Czechowski, N.; Lokstein, H.; Kowalska, D.; Ashraf, K.; Cogdell, R. J.; Mackowski, S. Large Plasmonic Fluorescence Enhancement of Cyanobacterial Photosystem Coupled to Silver Island Films. *Appl. Phys. Lett.* **2014**, *105*, 043701.
(20) Xu, H.; Aizpurua, J.; Käll, M.; Apell, P. Electromagnetic Contributions to Single-Molecule Sensitivity in Surface-Enhanced Raman Scattering. *Phys. Rev. E: Stat. Phys., Plasmas, Fluids, Relat. Interdiscip. Top.* **2000**, *62*, 4318−4324.
(21) Pilo-Pais, M.; Watson, A.; Demers, S.; LaBean, T. H.; Finkelstein, G. Surface-Enhanced Raman Scattering Plasmonic Enhancement Using DNA Origami-Based Complex Metallic Nanostructures. *Nano Lett.* **2014**, *14*, 2099−2104.
(22) Englebienne, P. Use of Colloidal Gold Surface Plasmon Resonance Peak Shift to Infer Affinity Constants from the Interactions between Protein Antigens and Antibodies Specific for Single or Multiple Epitopes. *Analyst* **1998**, *123*, 1599−1603.
(23) Nath, N.; Chilkoti, A. A Colorimetric Gold Nanoparticle Sensor to Interrogate Biomolecular Interactions in Real Time on a Surface. *Anal. Chem.* **2002**, *74*, 504−509.
(24) Haes, A. J.; Van Duyne, R. P. A Nanoscale Optical Biosensor: Sensitivity and Selectivity of an Approach Based on the Localized Surface Plasmon Resonance Spectroscopy of Triangular Silver Nanoparticles. *J. Am. Chem. Soc.* **2002**, *124*, 10596−10604.
(25) Antosiewicz, T. J.; Apell, S. P.; Claudio, V.; Käll, M. A Simple Model for the Resonance Shift of Localized Plasmons due to Dielectric Particle Adhesion. *Opt. Express* **2012**, *20*, 524−533.
(26) Zhang, W.; Martin, O. J. F. A Universal Law for Plasmon Resonance Shift in Biosensing. *ACS Photonics* **2015**, *2*, 144−150.
(27) Lee, K.-S.; El-Sayed, M. A. Gold and Silver Nanoparticles in Sensing and Imaging: Sensitivity of Plasmon Respones to Size, Shape, and Metal Composition. *J. Phys. Chem. B* **2006**, *110*, 19220−19225.
(28) Sekhon, J. S.; Verma, S. S. Refractive Index Sensitivity Analysis of Ag, Au, and Cu Nanoparticles. *Plasmonics* **2011**, *6*, 311−317.
(29) Nath, N.; Chilkoti, A. Label-Free Biosensing by Surface Plasmon Resonance of Nanoparticles on Glass: Optimization of Nanoparticle Size. *Anal. Chem.* **2004**, *76*, 5370−5378.
(30) Vörös, J. The Density and Refractive Index of Adsorbing Protein Layers. *Biophys. J.* **2004**, *87*, 553−561.
(31) Zeng, S.; Yong, K.-T.; Roy, I.; Dinh, X.-Q.; Yu, X.; Luan, F. A Review on Functionalized Gold Nanoparticles for Biosensing Applications. *Plasmonics* **2011**, *6*, 491−506.
(32) Dahlin, A. B.; Chen, S.; Jonsson, M. P.; Gunnarsson, L.; Käll, M.; Höök, F. High-Resolution Microspectroscopy of Plasmonic Nanostructures for Miniaturized Biosensing. *Anal. Chem.* **2009**, *81*, 6572−6580.
(33) Svedendahl, M.; Chen, S.; Dmitriev, A.; Käll, M. Refractometric Sensing Using Propagating versus Localized Surface Plasmons: A Direct Comparison. *Nano Lett.* **2009**, *9*, 4428−4433.
(34) Sannomiya, T.; Hafner, C.; Voros, J. In Situ Sensing of Single Binding Events by Localized Surface Plasmon Resonance. *Nano Lett.* **2008**, *8*, 3450−2455.
(35) Unger, A.; Rietzler, U.; Berger, R.; Kreiter, M. Sensitivity of Crescent-Shaped Metal Nanoparticles to Attachment of Dielectric Colloids. *Nano Lett.* **2009**, *9*, 2311−2315.
(36) Claudio, V.; Dahlin, A. B.; Antosiewicz, T. J. Single-Particle Plasmon Sensing of Discrete Molecular Events: Binding Position versus Signal Variations for Different Sensor Geometries. *J. Phys. Chem. C* **2014**, *118*, 6980−6988.
(37) Ament, I.; Prasad, J.; Henkel, A.; Schmachtel, S.; Sönnichsen, C. Single Unlabeled Protein Detection on Individual Plasmonic Nanoparticles. *Nano Lett.* **2012**, *12*, 1092−1095.
(38) Zijlstra, P.; Paulo, P. M. R.; Orrit, M. Optical Detection of Single Non-Absorbing Molecules Using the Surface Plasmon Resonance of a Gold Nanorod. *Nat. Nanotechnol.* **2012**, *7*, 379−382.
(39) Ahijado-Guzmán, R.; Prasad, J.; Rosman, C.; Henkel, A.; Tome, L.; Schneider, D.; Rivas, G.; Sönnichsen, C. Plasmonic Nanosensors for Simultaneous Quantification of Multiple Protein-Protein Binding Affinities. *Nano Lett.* **2014**, *14*, 5528−5532.
(40) Lüthgens, E.; Janshoff, A. Equilibrium Coverage Fluctuations: A New Approach to Quantify Reversible Adsorption of Proteins. *ChemPhysChem* **2005**, *6*, 444−448.
(41) Jokić, I.; Djurić, Z.; Frantlović, M.; Radulović, K.; Krstajić, P.; Jokić, Z. Fluctuations of the Number of Adsorbed Molecules in Biosensors Due to Stochastic Adsorption-Desorption Processes Coupled with Mass Transfer. *Sens. Actuators, B* **2012**, *166−167*, 535−543.
(42) Beuwer, M. A.; Prins, M. W. J.; Zijlstra, P. Stochastic Protein Interactions Monitored by Hundreds of Single-Molecule Plasmonic Biosensors. *Nano Lett.* **2015**, *15*, 3507−3511.
(43) Sekhon, J. S.; Verma, S. S. Optimal Dimensions of Gold Nanorod for Plasmonic Nanosensors. *Plasmonics* **2011**, *6*, 163−169.
(44) Squires, T. M.; Messinger, R. J.; Manalis, S. R. Making it stick: Convection, Reaction and Diffusion in Surface-Based Biosensors. *Nat. Biotechnol.* **2008**, *26*, 417−426.
(45) Salary, M. M.; Mosallaei, H. A Quasi-Static Continuum Model Describing Interactions between Plasmons and Non-Absorbing Biomolecules. *J. Appl. Phys.* **2015**, *117*, 234303.
(46) Kaizu, K.; de Ronde, W.; Paijmans, J.; Takahashi, K.; Tostevin, F.; ten Wolde, P. R. The Berg-Purcell Limit Revisited. *Biophys. J.* **2014**, *106*, 976−985.
(47) Häfele, V.; Trügler, A.; Hohenester, U.; Hohenau, A.; Leitner, A.; Krenn, J. R. Local Refractive Index Sensitivity of Gold Nanodisks. *Opt. Express* **2015**, *23*, 10293−10300.
(48) Leitgeb, V.; Trugler, A.; Kostler, S.; Krug, M. K.; Hohenester, U.; Hohenau, A.; Leitner, A.; Krenn, J. R. Three Dimensional Sensitivity Characterization of Plasmonic Nanorods for Refractometric Biosensors. *Nanoscale* **2016**, *8*, 2974−2981.
(49) Caswell, K. K.; Wilson, J. N.; Bunz, U. H. F.; Murphy, C. J. Preferential End-to-End Assembly of Gold Nanorods by Biotin-Streptavidin Connectors. *J. Am. Chem. Soc.* **2003**, *125*, 13914−13915.

DOI: 10.1021/acs.jpcc.6b01897
J. Phys. Chem. C 2016, 120, 20692−20701

(50) Beeram, S. R.; Zamborini, F. P. Selective Attachment of Antibodies to the Edges of Gold Nanostructures for Enhanced Localized Surface Plasmon Resonance Biosensing. *J. Am. Chem. Soc.* **2009**, *131*, 11689−11691.

DOI: 10.1021/acs.jpcc.6b01897
J. Phys. Chem. C 2016, 120, 20692−20701